Density-Functional Tight-Binding Simulations Reveal the Presence of Surface Defects on the Quartz (101)-Water Interface

Ke Yuan[1*], Nikhil Rampal[2], Paul Fenter[3], James D. Kubicki[4], Andrew G. Stack[1], Stephan Irle[5*]

1. Chemical Sciences Division, Oak Ridge National Laboratory, Oak Ridge, TN 37831
2. Department of Chemical Engineering, Columbia University, New York, NY 10027
3. Chemical Sciences and Engineering Division, Argonne National Laboratory, Lemont, IL 60439
4. Department of Geological Sciences, The University of Texas at El Paso, El Paso, TX 79968
5.Computational Sciences and Engineering Division, Oak Ridge National Laboratory, Oak Ridge, TN 37831

Corresponding Authors: Ke Yuan, Email: yuank@ornl.gov, phone: 865-576-7184; Stephan Irle, Email: irles@ornl.gov, phone: 865-574-7192

Abstract

Understanding the structure and reactivity of quartz-water interfaces is critical for numerous applications in the geological, environmental, and biological sciences. However, disagreements on the atomic-level structure of the interfaces between experiments and simulations are hampering our ability to predict the surface reactivity. Here, we used density-functional tight-binding (DFTB)-based molecular dynamics to simulate a series of quartz (101) surfaces having different types and densities of surface defects in water and compared them with the structures determined by X-ray reflectivity measurements. The DFTB simulations are able to reproduce previous classical and quantum mechanical predictions of the pristine quartz (101)-water interface that disagree with experimental observations. To remedy this situation, a set of defective quartz surfaces having various surface silicon (Si) vacancies were built as indicated by recent experimental studies. We found that the rotation of surface [SiO_4] tetrahedra near Si vacancies can lead to outward displacements of Si atoms similar to those observed in the experiments. The presence of additional surface Si vacancies caused inward relaxations of terminal oxygens through the formation of hydrogen bonds. The overall results indicate that the quartz (101)-water interface

may include a mixture of geminal (≡ Si-$(OH)_2$) and vicinal (≡ Si-OH) type silanol groups together with the presence of surface Si vacancies.

Introduction

Quartz is a common mineral phase that contributes to a major portion of the Earth crust and is an important material used in the construction industry and in analytical chemistry[1-3]. Understanding the structure and dynamics of hydrated quartz surfaces is crucial for a wide spectrum of fundamental processes, such as dissolution/growth of silicates, uptake/release of toxic metals in subsurface environments, biosensing, and surface catalysis[4-7]. The surface charge of quartz plays a central role in interfacial reactions, intimately linked to the dynamic structure of surface silanol (≡Si-OH) groups[8]. Tuning of the surface charge can be achieved by protonation/deprotonation of hydroxyl groups at the silanol sites[9]. Second harmonic and sum frequency generation (SHG, SFG) measurements have revealed the presence of two different surface silanol groups with acidities of pK_a = 4.5 and pK_a = 8.5, respectively, on both amorphous silica and quartz (100) surfaces[10-12]. First principles density functional theory (DFT)-based molecular dynamics (MD) simulations equally observed two types of hydrogen-bonding environments for silanol groups on the quartz (100) surface, and the computed water vibrational modes and pK_a values were close to experimental measurements[13-14]. However, in an alternate set of simulations, the more acidic surface silanol groups of pK_a = 4.5 were interpreted as belonging to defective, strained areas of the surface that contained fewer silanol groups[15].

Despite ongoing research activities aimed at clarifying the origin of bimodal surface acidities of quartz, it is surprising that the structure of the quartz surface in water remains poorly understood. Discrepancies between experimental structural data and theoretical predictions have thus far not been resolved[16-17]. In 2015, X-ray reflectivity crystal truncation rod (CTR) measurements were used to characterize the atomic-scale structure of the quartz (101) surface *in situ* in water, revealing significant discrepancies in the positions of terminal oxygen (O) atoms between the measured and calculated quartz (101)-water interface structures[18]. The CTR experiments found that the surface O atoms associated to surface hydroxyls relaxed (with respect to bulk-like quartz) in an inward direction (towards the quartz surface substrate) by of −0.25 ± 0.02 Å, whereas the MD and DFT-based MD (DFT/MD) calculated structures all showed an outward shift toward the solution[16, 18].

There is also a significant amount of theoretical work performed on simulating the structure and energetics of quartz (100) surface in water and in various electrolytes[14, 19-20]. Here, we focused on comparing experimental and computational data of the quartz (101) surface.

This work focuses on the applicability of the computationally economical density-functional tight-binding (DFTB) method and its predictions regarding the solvated quartz (101) surface. DFTB is a semiempirical quantum chemical method that uses an approximate Kohn-Sham density functional theory (KS-DFT) with an linear-combination-of-atomic-orbitals (LCAO) representation of the Kohn-Sham (KS) orbitals[21]. The DFTB method is based on parameterized Hamiltonian and basis set overlap matrix elements, and in principle maintains *ab initio* DFT accuracy in its predictions while achieving the computational speed of semiempirical tight-binding (TB) methods[22-23]. These advantages allow DFTB/MD simulations of up to 26 defective structures on time scales from 25 ps to 160 ps with simulation cells composed of 500 atoms to ~2000 atoms. We first establish the accuracy of the DFTB method for the silica-water interface by comparing predicted interface structures against DFT and high quality experimental CTR data measured from this surface termination[14, 19-20]. We then investigate defective surface models, as we noticed that previous X-ray reflectivity data suggested missing Si atoms in the outermost layer of a quartz surface[16]. Finally, we simulate our most likely candidate structures in large supercells (~2000 atoms) in order to investigate size effects on the calculated structures.

Computational Methods

DFTB/MD

The DFTB+ program was used in MD and metadynamics (MTD) canonical simulations in the NVT ensemble of the quartz (101)-water interface in a unit cell with 3D periodic boundary conditions (PBC)[24]. We selected the third-order DFTB (DFTB3) flavor which includes the fluctuation of chemical hardness with atomic charge, in conjunction with the 3ob (Third-Order Parametrization for Organic and Biological Systems) parameterization[25]. Brillouin zone sampling was performed with a selection of 3×3×3 k points for structure optimizations and a Γ point selection for MD simulations. Time integration was carried out with a time step of 0.4 fs and the temperature was maintained using 298.15 K as target temperature for the Nose-Hoover thermostat. Defective quartz surface models were created by removing selected Si atoms and the broken bonds were saturated with hydrogen. The pbc (Periodic Boundary Condition) parameterization was used

for the geometry optimization of the α-quartz and the results were compared with that obtained by matsci (Materials Science) parameterization and DFT[26-28]. Quartz structures optimized with the pbc parameterization were closest to experimental data in terms of unit cell lengths and Si-O-Si bond angles (Table S1). For the simulation of water, we used the previously developed 3obw parameterization[29], which was designed to reproduce the experimental radial distribution function (RDF) of water (Figure S1). Details of the simulation parameters are given in the Supporting Information.

Quartz surface model

The quartz (101) surface containing 6 O-Si-O layers was cleaved from an optimized bulk α-quartz supercell. The top layer of the quartz (101) surface was allowed to relax while the bottom 5 layers were fixed during the MD simulations to maintain a bulk-like structure. This methodology has been shown to yield best results in terms of reproducing the experimental geometry of the quartz surface in previous studies[16,18]. The charge-neutral surface was modeled with hydroxyl terminations. The quartz (101) surface is terminated by vicinal (Q^3) type silanol groups, where two ≡Si-OH sites share a common oxygen vertex (Figure 1a). There are two silanol (≡Si-OH) groups at slightly different heights above the quartz (101) surface, where the O atoms are labeled as O5 (inner) and O6 (outer) in Figure 1a following conventions from previous studies[16-18]. The surface model has dimensions of a = 9.94 Å, b = 13.92 Å, and c = 42.07 Å with a chemical formula of $Si_{72}O_{244}H_{200}$, which includes 92 water molecules filled in a 20-Å-high vacuum space maintaining a bulk water density close to 1.0 g/cm^3. The $2 \times 1 \times 1$ and $2 \times 2 \times 1$ supercells were used to simulate the pristine and defective structure that showed closest match with the experimental data.

Results

Structure of the pristine quartz (101)-water interface

The first step to examine the differences between computational results and experimental data on the quartz (101)-water interface is to compare the calculated and measured surface atom displacements. Previous X-ray reflectivity measurements had been performed on four quartz (101) samples, all obtained as natural quartz minerals from Herkimer County, New York[16-17]. Prior to those experiments, the quartz samples had all been washed by solvents (methanol and water) and treated with slightly different methods (Table 1). The X-ray data by Bellucci et al.[16] were measured

up to a higher Q value (i.e., Q_{max} = 5.5 Å^{-1}) and thereby determined with a higher spatial resolution (π/Q_{max} = ~1.1 Å) compared to those by Schlegel et al.[17] (Q_{max} = 4.2 Å^{-1} and the spatial resolution of 1.5 Å, respectively). Nonetheless, both measurements showed similar displacements of surface O and Si atoms, in terms of the direction as well as the magnitudes, with those by Bellucci et al. having smaller uncertainties of estimation for O5 and O6 atoms (Figure 1b).

Experimental CTR data showed that the Si3 atoms relaxed +0.17 Å (towards the direction of the solution) and both O6 and O5 atoms relaxed significantly into the crystal by –0.25 Å and –0.15 Å (Figure 1b), respectively, whereas the DFTB-simulated quartz (101) surface showed no major relaxations (Figure 1c). Previous calculated quartz (101)-water structures all showed positive shifts in O6 and O5 atoms (Figure 1c). Our DFTB calculated displacements were similar to that obtained by DFT (Bellucci et al.) and MD simulation using CWCA (Combinatorial Week-Chandler Andersen) potentials. Of special note, DFTB systematically overestimated the quartz lattice constants by about 1.1% (Table S1), which can impact the comparisons between simulated and experimental surface structures. We corrected this error by scaling down the DFTB calculated atom positions before the calculation of displacements. In order to test whether fixing the bottom five O-Si-O layers in our model will induce strain and surface structure changes, we allowed the top three O-Si-O layers instead of the top one layer to relax in the DFTB/MD simulation. The displacements of Si, O6, and O5 atoms in the top surface of the three relaxed layers were similar to those calculated in the model by allowing the relaxation of the top one layer (Figure S2). Thus, the top one-layer relaxed model was used here.

Second, we compared the DFTB calculated electron density profile to experimental results. The electron density profiles measured by X-ray reflectivity taking into account the finite resolution of the CTR measurements, the peak heights and peak widths may not be directly comparable to DFTB results. Instead, we focused on the comparisons of peak positions and the derived water occupation numbers. Here, we defined the averaged positions of Si atoms in the 2nd O-Si-O layer (position fixed during simulation) as zero and reported all measured distances with respect to this reference point (Figure 1a and Table 1). The DFTB calculated electron density profile had similar positions for the first and second O-Si-O layers compared to the experimental data but disagrees on the positions of adsorbed water and terminal oxygens (Figure 1a). The CTR measured by Bellucci et

al. revealed a first adsorbed water layer at 6.69 ± 0.01 Å with a corresponding water occupation of 0.12 water/Å^2. The CTR measured by Schlegel et al. showed an adsorbed water at 6.6 Å to 7.5 Å and a water occupation ranging from 0.05 to 0.07 water/Å^2 for three different samples. The DFTB calculated structure showed that the absorbed water was located at 7.35 Å. Three Gaussian peaks were used to fit the water profile, yielding an integrated area of 0.44 e^-/Å^2 for adsorbed water, equivalent to a water occupation of 0.044 water/Å^2 (Table 1 and Figure S3). We performed additional simulations of the pristine quartz (101) surface in two larger supercells (Figure 1d). In all cases, the results showed little changes in the position of the adsorbed water with a bulk water electron density close to 0.33 e^-/Å^3. Minor ordering of water further from the first water layer was observed in the 2 × 2 × 1 supercell (Figure 1d). In general, the atom displacements and electron density profiles together indicated that the precise atom locations in the quartz (101)-water interfacial model obtained from a bulk-like termination appear to be inconsistent with the experimental observations and their uncertainties.

Table 1. Summary of published X-ray reflectivity measurements on the quartz (101)-water interface.

Sample	Sample treatment	Adsorbed water position* (Å)	water occupation (water/Å^2)
Annealed_Bellucci 2015	400°C for 12 h	6.69	0.12
Annealed_Schlegel 2002	400°C for 48 h	6.85	0.05
Natural 1_ Schlegel 2002	Kept in water for 10 months	6.59	0.07
Natural 2_ Schlegel 2002	In air	7.50	0.06
Pristine (DFTB)	--	7.35	0.04

* Refer to the averaged positions of Si atoms in the 2nd O-Si-O layer as zero

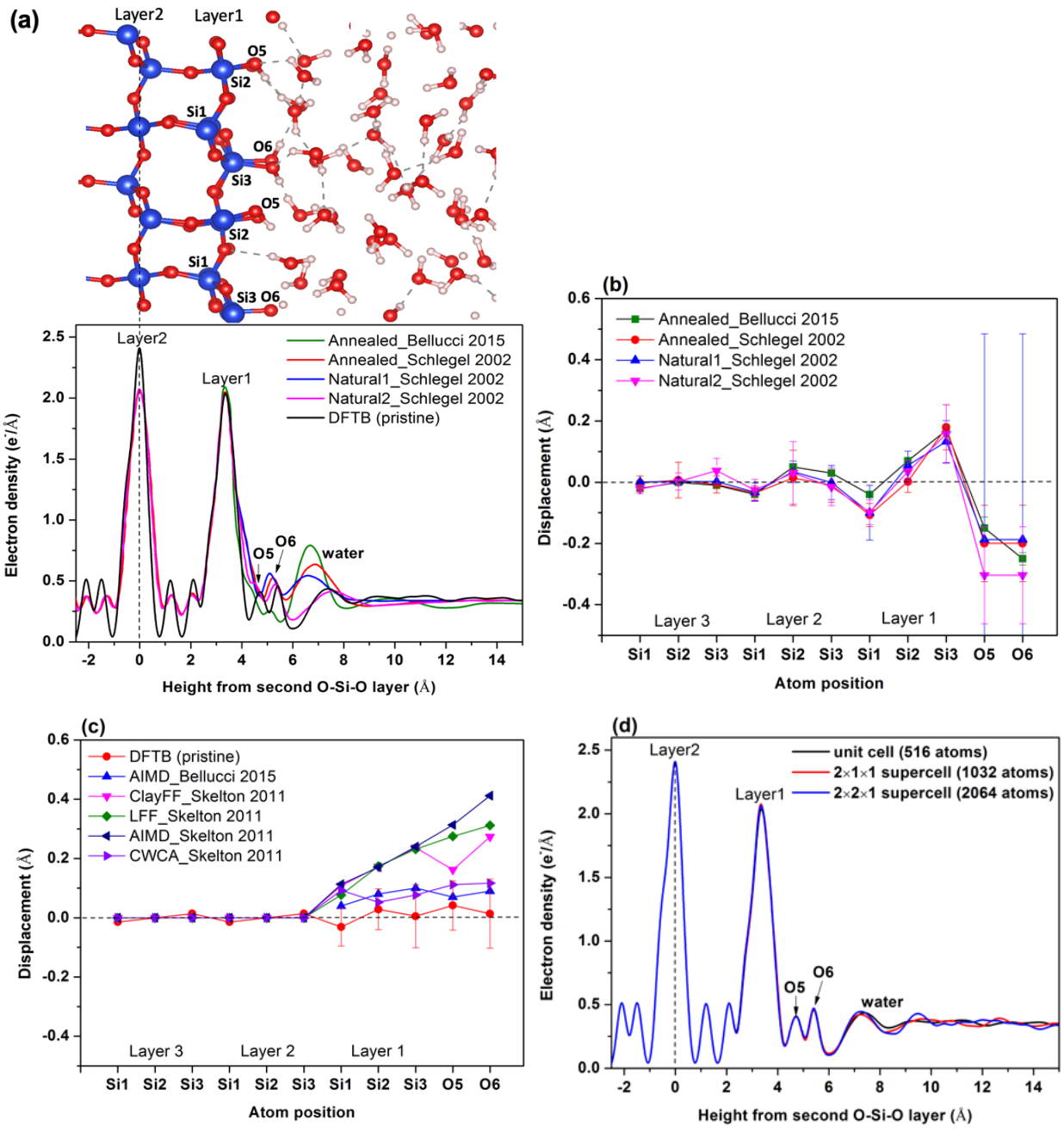

Figure 1. (a) Comparison between the DFTB-calculated and the experimentally measured electron density profiles along the surface normal direction. The interfacial structure model is shown on top, where the O and Si atoms at different surface heights are labeled. Vertical relaxations of top three O-Si-O layer of the quartz (101) surface in water measured by (b) X-ray reflectivity and (c) calculated by using computational methods[16-17]. Error bars in DFTB/MD calculated displacements in (c) are 1-sigma standard deviations from averaged atom positions over 160 ps of MD simulation. (d) Electron density profiles obtained based on DFTB/MD simulations in a unit cell (160 ps), 2 × 1 × 1 supercell (40 ps), and 2 × 2 × 1 supercell (30 ps).

Quartz (101) surface with various types of Si vacancies

The calculated pristine quartz (101)-water interface showed major discrepancies relative to experimental results (Figure 1a). To shed further light on this topic, we constructed defective quartz (101) surface structures based on fitted Si occupancies to CTR data[16]. There are three unique types of Si (Si3, Si2, and Si1 in Figure 1a) located at different heights of the top O-Si-O layer. The experimental CTR data had shown that about 30% of Si3 atoms were missing in the top O-Si-O layer. Our model contains in total of 12 Si atoms in the top layer (four atoms per each type of Si). Removing one of the four Si3 atoms created a 25% Si3 vacancy. We have also explored other structures containing 25% Si1 and 25% Si2 vacancies, structures containing 50% of either Si1, Si2 or Si3 vacancies, and structures containing a mixture of two types of Si vacancies (25%Si1+25%Si2, 25%Si1+25%Si3, and 25%Si2+25%Si3). Si vacancy was manually created by removing a Si atom and protonating the nearby $\equiv$Si-O$^-$ sites (or associated -OH group to form water) to balance the charge. All Si vacancy-bearing structures were first optimized in vacuum prior to exposure to water. We found Si3 atoms in the top layer showed positive shifts in models with 25% Si1- and Si2-type vacancies similar to that measured by CTR, but the terminal O5 and O6 positions remained unchanged (Figure 2a). Electron density profiles of all 25% Si vacancy-bearing structures had no significant changes in peak positions with minor changes in peak heights (Figure 2b). In a pristine quartz (101) surface, all surface [SiO_4] tetrahedrons associated with Si3 atoms were terminated with a single -OH group (Q^3, vicinal type silanol) as shown in Figure 1a. In the structure with a Si1- or Si2-type vacancy, a [SiO_4] tetrahedron near the vacancy site was found to be terminated by two -OH groups (Q^2, geminal type silanol). This type of surface units is shown in the orange color in Figure 3a, and 3b and is not observed in the structure with Si-3 type vacancy (Figure 3c). The Si vacancy formation generated one additional -OH group attached to the [SiO_4] tetrahedron and allow the tetrahedron to rotate with two -OH pointing towards the solution in MD simulations. This type of rotation was responsible for the positive shifts of the associated Si3 atoms (Figure 3d). We further made 6 additional structures, each containing 50% of either Si1, Si2, or Si3 vacancies and a mixture of two types of Si vacancies. Geminal silanol groups with positive Si3 shifts were found in structures that contain a single rotation of surface [SiO_4] (Figure S4 and S5). We calculated the vacancy formation energies on various types of defective quartz surfaces by calculating the energy differences to reference models of the same compositions balanced by $[SiOH_4]_{(aq)}$ and H_2O (see an example of a reference model in Figure

S6). To be noticed, these energy calculations were not aimed to compute the exact free energy of formation but rather provided a qualitative understanding on the relative stability of various Si defects could be formed on the quartz (101) surface. The results indicated the formation of Si3 type vacancy were energetically more favorable and the energy costs increased with increasing number of Si vacancies on the surface (Figure 4). We have also investigated two other types of surface defects, namely, O vacancies and edge-shared [SiO_4] tetrahedra as indicated by previous experimental studies[30]. All structures with O vacancies were unstable in water and restored to a pristine quartz surface structure due to the high reactivity of $\equiv$Si-O^+ site associated with the O vacancy (Figure S7). Structures with edge-shared [SiO_4] tetrahedra on the surface showed negative shifts on the surface Si3 atoms which are inconsistent with experimental X-ray reflectivity results (Figure S8). Thus, it is necessary to investigate the effect of the rotation of surface [SiO_4] tetrahedrons on the displacements of surface Si3 atoms.

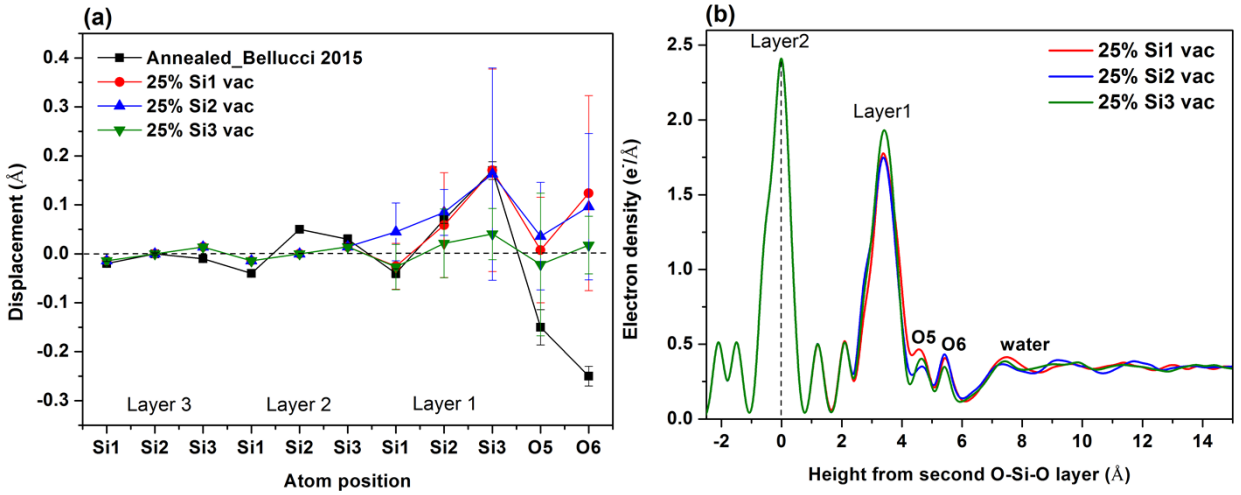

Figure. 2 (a) Vertical relaxations of the atoms in the defective quartz (101)-water interface having a 25% vacancy in one of the three types of Si atoms (Si1, Si2, or Si3). (b) Electron density profiles of these 25% Si vacancy-bearing structures obtained based on 30 ps of DFTB/MD simulations.

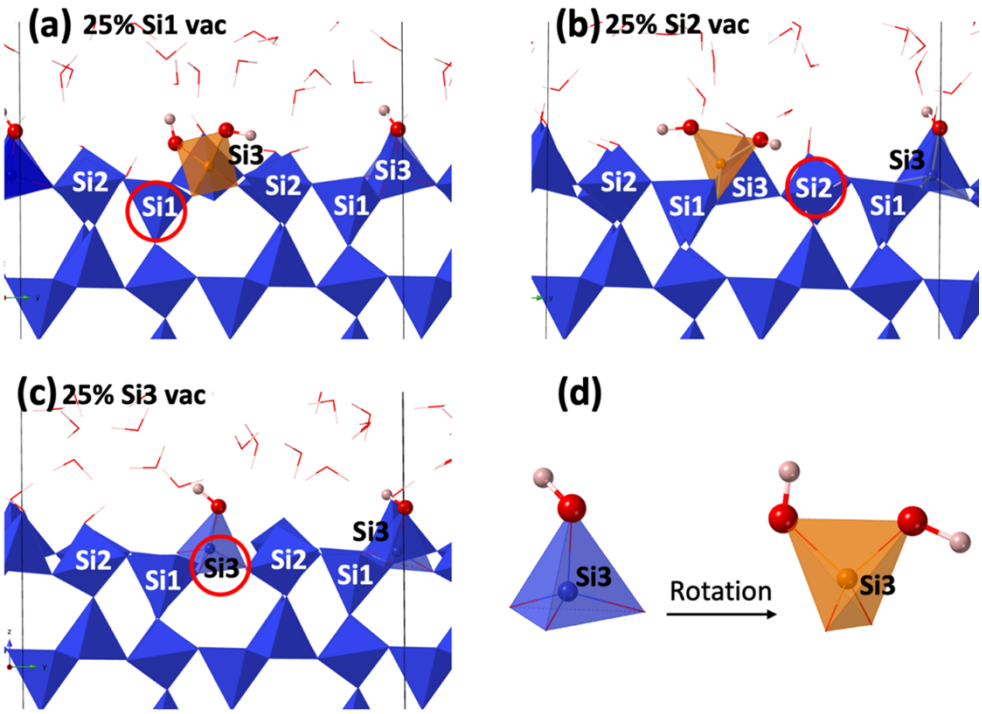

Figure. 3 Snapshots from DFTB/MD simulations showing quartz (101)-water interfaces having (a) 25% Si1, (b) 25% Si2, and (c) 25% Si3 vacancy. Red circles indicate the locations of Si vacancies. (d) Rotation of a single -OH terminated [SiO_4] tetrahedron found on pristine quartz surface leads to a double hydroxyl terminated silanol group.

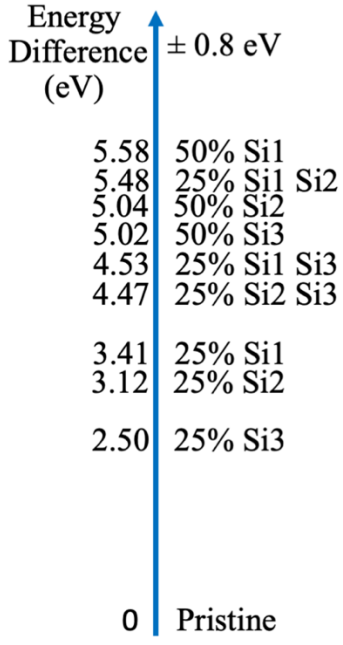

Figure. 4 Energies of formation of different types of Si vacancies on the quartz (101) surface in water ± 0.8 eV is the standard deviation calculated based on energies over 1 ps in DFTB/MD simulations.

Quartz (101) surface with rotation of [SiO_4] tetrahedra

Based on results showed in the previous section where a strong correlation between rotated surface [SiO_4] and negative displacements in Si3 atoms were observed, we created a series of models containing different numbers of rotated surface [SiO_4] tetrahedra without Si vacancies (Figure 5). The displacements of Si3 atoms in the top Si-O-Si layer increased from about +0.1 Å to +0.5 Å with the increased rotation of 25% to 100% [SiO_4] tetrahedrons (Figure 5a, 5c, and 5d). In comparison, the positions of O5 and O6 atoms remain unchanged. The electron density profiles showed an increase in peak height at about 4.2 Å, corresponding to the positive shifts of Si3 atoms inside the [SiO_4] tetrahedrons (Figure 5b). The O5 peaks became invisible on the electron density profiles due to their overlap with peaks from Si3, and positions of the O6 peak remained unchanged. The positions of the adsorbed water have +0.9 Å shifts away from the quartz surface in structures containing 75% and 100% [SiO_4] rotation. The displacements of the Si3 atoms in these two structures were also too large compared with experimental data. Thus, it is likely that rotation of 25% to 50% of surface [SiO_4] groups was ideal to have about +0.2 Å shifts on Si3 atoms. However, additional structure modifications were required in order to impact the positions of O6 and O5 atoms.

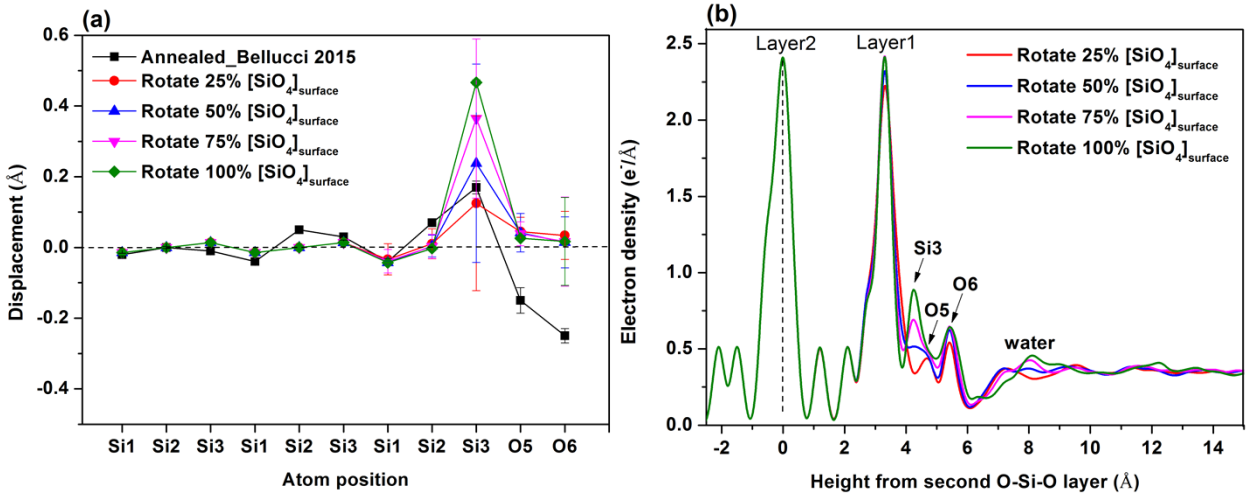

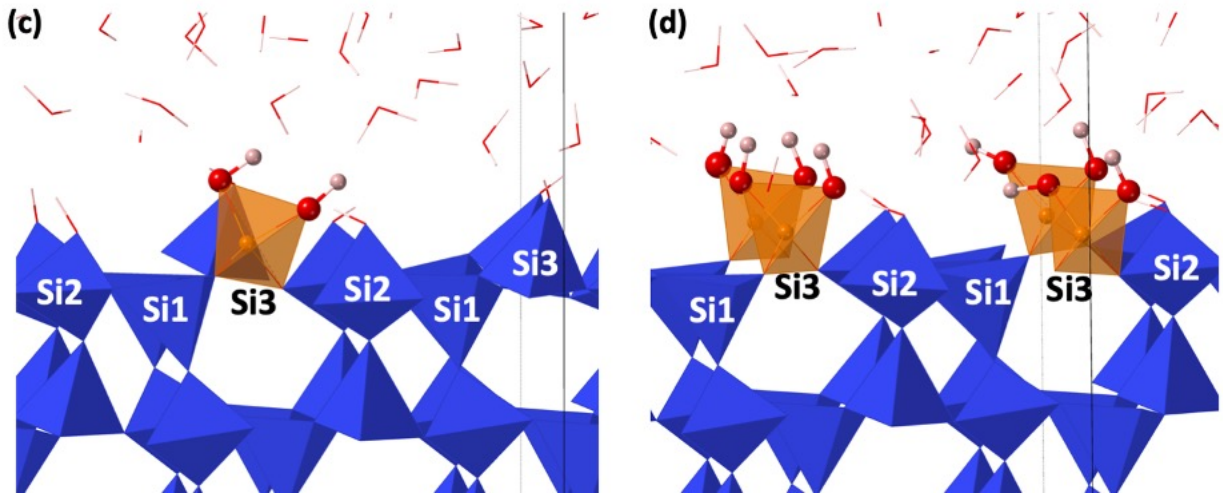

Figure 5. Rotation of different portions of surface [SiO_4] tetrahedra associated with Si3 atoms on the (a) atom displacements (b) electron density profiles of quartz (101)-water interfaces calculated from 70 ps of DFTB/MD simulations. Snapshots from DFTB/MD simulations showing (c) rotation of 25% surface [SiO_4] and (d) rotation of 100% surface [SiO_4].

Quartz (101) surface with [SiO_4] rotation and Si3 vacancies

Based on the previous analysis, the rotation of surface [SiO_4] associated with Si3 atoms without Si vacancies can create desired positive shifts on Si3 atoms. Structures with 25% and 50% [SiO_4] rotation matched better to the CTR data in terms of the Si3 positions. Thus, we increased the amount of Si3 vacancies in these two structures in order to investigate the Si vacancy effects. The reason of not creating Si1 or Si2 vacancies is because the [SiO_4] tetrahedron is corner shared with two nearby tetrahedrons associated with Si1 or Si2 atoms (Figure 3). Removing either Si1 or Si2 atom will break the stable corner-sharing structure leaving a triple hydroxyl terminated [SiO_4] unit. In addition, Si3 vacancies were energetically more favorable to form than Si1 and Si2 vacancies (Figure 4).

In the structures with 25% rotation of surface [SiO_4] groups, negative shifts of O5 atoms were observed in all Si3 vacancy bearing structures (Figure 6a). Negative shifts of O6 atoms were observed in structures containing more than 25% Si3 vacancies. The electron density profiles showed corresponding shifts of O5 peaks by about -0.2 Å in all structures and shifts of O6 peaks by -0.1 Å in structures with 50% and 75% Si3 vacancies (Figure 6b). In another set of structures with 50% [SiO_4] rotation, negative shifts of O6 and O5 were observed in the structure containing

50% Si3 vacancies. However, the electron density profile showed less obvious changes on the position of O6 peak due to large uncertainties in the estimated displacements (Figure S9). The positions of the adsorbed water showed small variations in all structures (Figure S9).

We found two candidate structures showing similar displacements of surface atoms compared to the experimental data (Figure 6c). Both structures contained 50% Si3 vacancies but varied in the portion of [SiO_4] rotation. Their electron density profiles matched that of the Natural 2 quartz sample measured by Schlegel et al. in terms of the peak positions (Figure 6d). The O5 peak positions in the candidate structures were similar to that measured by Bellucci et al., but the positions of O6 and the adsorbed water had significant differences. The structure with 25% rotation of surface [SiO_4] and 50% Si3 vacancies matched best to the Natural 2 quartz sample in terms of the atom displacements (especially Si3 and O5) and electron density profile. We therefore performed an additional simulation of this structure in a $2 \times 2 \times 1$ supercell (Figure 7a and 7b). A close analysis on this structure revealed unique H-bond environments near the rotated [SiO_4] tetrahedrons (Figure 7b). We found the O6 atoms associated with [SiO_4] formed hydrogen-bonds (H-bonds) with nearby -OH groups due to the Si3 vacancy formation. These -OH groups were attached to Si1 atoms that were lower in height than Si2 and Si3 atoms (Figure 7c). The attraction from these underneath -OH groups forced the surface O6 and O5 atoms to move inward, leading to the negative shifts observed in atom displacements and peak positions. Four H-bonds responsible for the negative shifts were labeled in Figure 7b with the corresponding bond lengths plotted over time (Figure 7c). OH1 and OH4 which were responsible for the inward shifts of O6 and O5 atoms, respectively, showed shorter bond lengths (Figure 7e) and less fluctuations (Figure 7d) than that of OH2 and OH3, indicating a more stable H-bond environments.

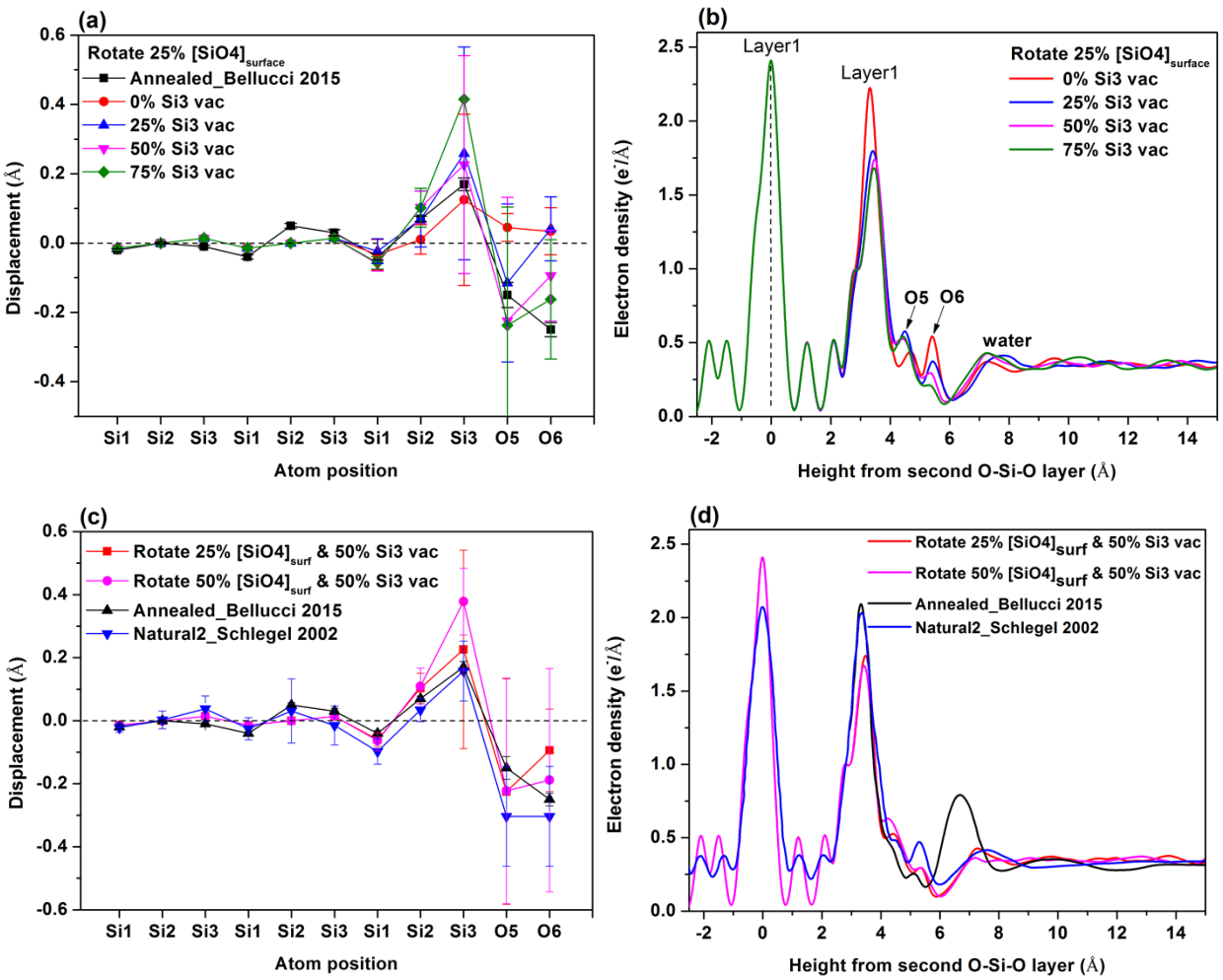

Figure 6. (a) Vertical relaxations of defective quartz (101) surface with 25% rotation of surface [SiO_4] groups together with increasing amount of Si3 vacancies. (b) Electron density profiles of corresponding structures based on 70 ps of DFTB/MD simulations. (c) Vertical relaxation and (d) electron density profiles of two candidate structures compared to experimental results.

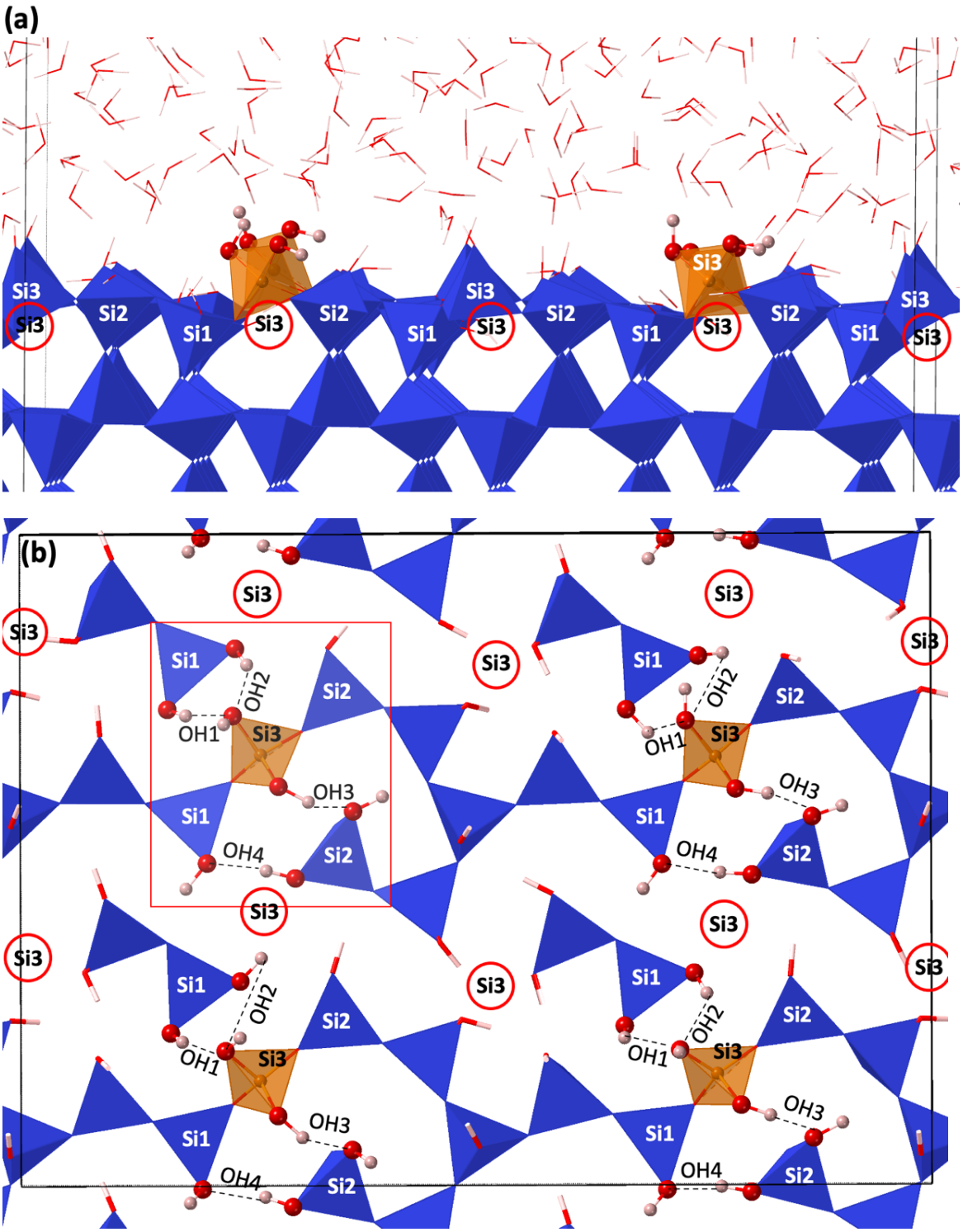
(a)
Si3
Si2
Si1
(b)
OH1
OH2
OH3
OH4

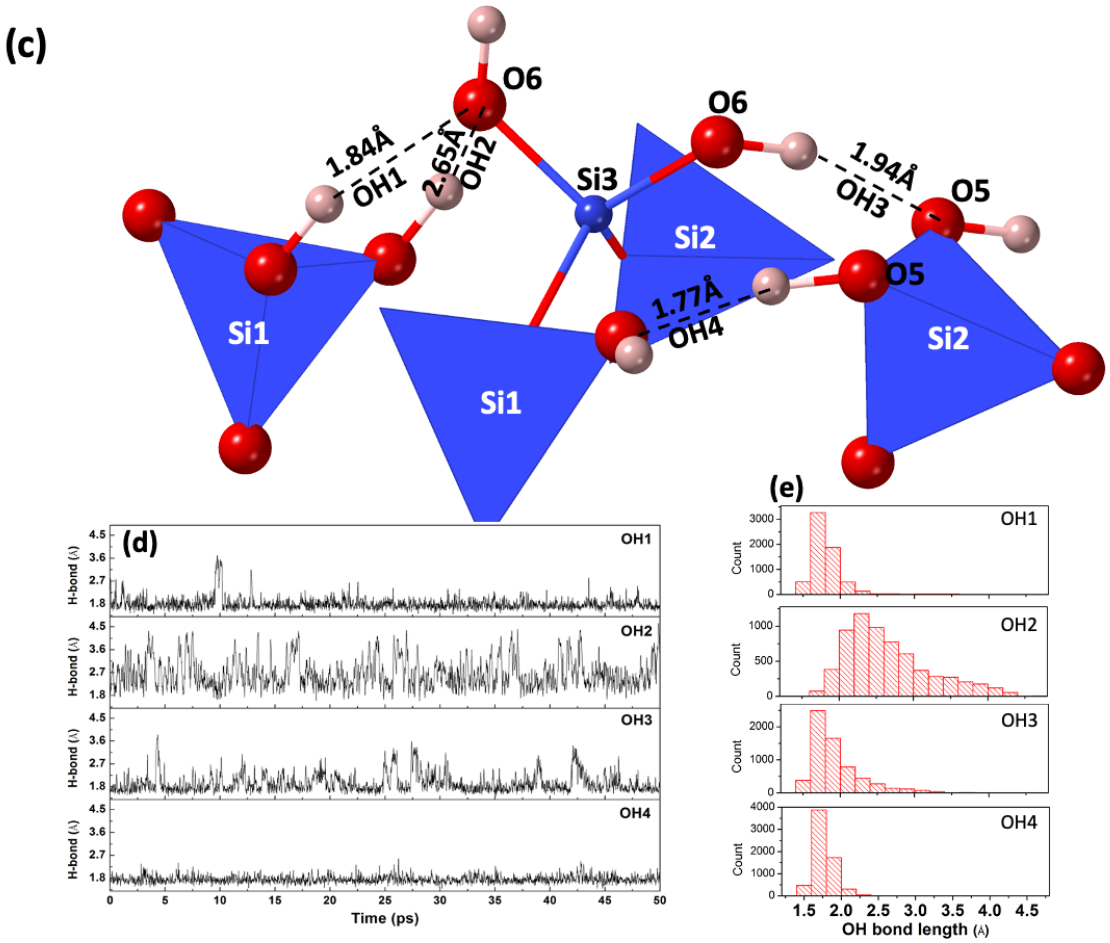

Figure 7. (a) Side and (b) top views of the snapshots from DFTB/MD simulation of the quartz (101) surfaces with 25% rotation of surface [SiO_4] and 50% Si3 vacancies. The rotated [SiO_4] groups are in orange and the location of Si3 defects were labeled by red circles. (c) A close view inside the box labeled in (b) showing 4 H-bonds (OH1, OH2, OH3, and OH4) responsible for inward shifts of O6 and O5 atoms. The average bond lengths were labeled with the (d) showing bond lengths changing over time and (e) showing the corresponding distributions of OH bond lengths in histograms.

Discussion

Fitted occupancies to CTR data suggested that the quartz (101) surface may contain a surface layer with reduced electron density, which motivated us to explore computationally possible surface defects. Comparison of CTR data with computational results has been used to study other solid-water interfaces, such as calcite ($CaCO_3$)[31], rutile (TiO_2)[32], corundum (Al_2O_3)[33], barite ($BaSO_4$)[34] and xenotime (YPO_4)[35]. Quartz surfaces are challenging to measure by CTR because quartz has

poor cleavage planes, whereas such measurement usually require atomically flat surfaces. Quartz surfaces can readily become amorphous and contaminated by mechanical polishing[16-17]. Silica materials and silicate minerals are known to have various surface defect sites, such as Si and O vacancies, non-bridging O, impurity cation substitution sites, and peroxy linkage site (Si-O-O-Si)[36-38]. In particular, the quartz (101) surfaces used for all CTR measurements were natural growth surfaces. The samples were either annealed, left in water for 10 months, or stored in air before the experiments. These different sample preparation methods may lead to changes to the surface structure, which can lead to the observed differences in electron density profiles. So far, only specular CTR signals from the quartz (101) surfaces have been collected, which are sensitive to atomic relaxations along the surface normal to the surface direction. To gain full insights into the surface structure, non-specular CTR data will be needed, which can be used to establish lateral movements of surface atoms[39].

Experimental CTR data from Bellucci et al showed a peak of higher water occupation number (Table 1). This has been attributed to possible formation of defective SiO_2 layer with partial surface coverage. Since quartz does not have perfect cleavage planes, the (101) surface prepared by different groups used for CTR measurements may vary in surface defect density and surface terminations. These will impact the surface hydroxyl group distribution, therefore, the position and occupation of adsorbed water above the surface. Despite the possible variations in quartz (101) surface, all CTR data measured in 4 samples by two different groups showed similar displacements on Si3 and O6 and O5, indicating there are intrinsic features that are general to the quartz (101) surface termination.

The candidate structures showed that the rotation of surface [SiO_4] unit can lead to positive shifts of Si3 atoms. Rotation of more than 50% [SiO_4] yielded too much positive shifts. The pristine quartz (101) surface is covered with all single hydroxyl terminated silanol groups (≡ Si-OH). This correlation indicates that the quartz (101) surface may contain a mixture of single (Q^2) and double hydroxyl terminated (Q^3) silanol groups. This configuration is different from those assumed in previous CTR and computational simulations, which all indicated a bulk-like termination with single hydroxyls. In addition to [SiO_4] rotation, the H-bond formation was critical for pulling terminal O atoms toward the quartz surface. New -OH groups were formed on [SiO_4] tetrahedrons

associated with Si1 atoms in the vicinity of Si3 vacancies, and they were primarily bond with -O(6)H and -O(5)H hydroxyls on the top surface. Because these underneath -OH groups do not form the H-bond with water, the peak height of adsorbed water on the electron density profiles showed no significant change (Figure 6b). Instead, the H-bond formation between top layer -O(6)H/-O(5)H and water is responsible for the electron density of the adsorbed water layer. Our calculated water occupation number was about 60% smaller than the experimental value reported by Bellucci et al. (2015)[16]. This could be due to that the quartz (101) surface measured by Bellucci et al. may contain adsorbed cations bringing additional hydration shells close to the quartz surface or could be due to the presence of a partial SiO_2 layer on the surface.

Conclusions

DFTB method was used to efficiently investigate the structure of a series of quartz (101) surfaces having various types and densities of surface defects (i.e., 26 models in total) in water which allowed fast screen of candidate structures. Our results showed that the DFTB calculated pristine quartz (101)-water interface is similar to those reported previously by DFT and MD. We found the presence of Si3 vacancies leading to double hydroxyl terminated silanol groups on quartz (101) surface can partially resolve the discrepancies between experimental and computational results. Si vacancies could potentially impact the deprotonation energies of surface -OH groups, which are subject to further investigations.

Supporting Information

Computational Details on the DFTB Calculations; Vertical relaxations and electron density profiles of defective quartz (101) surface with 50% Si1, Si2, or Si3 vacancy; Vertical relaxations and electron density profiles of defective quartz (101) surface with a mixture of either 25% of Si1Si2, Si1Si3, or Si2Si3 vacancies; A reference model used for energy difference calculation; Vertical relaxations and electron density profiles of the calculated defective quartz (101) surfaces containing various O vacancies and an edge-shared [SiO_4] defective surface; Vertical relaxations and electron density profiles of defective quartz (101) surface with 50% rotation of surface [SiO_4] groups together with increasing amount of Si3 vacancies.

Acknowledgement

This work is supported by the U.S. Department of Energy, Office of Science, Office of Basic Energy Sciences, Chemical Sciences, Geosciences, and Biosciences Division. This research used resources of the National Energy Research Scientific Computing Center (NERSC), a U.S. Department of Energy Office of Science User Facility operated under Contract No. DE-AC02-05CH11231. This research used resources of the Compute and Data Environment for Science (CADES) at the Oak Ridge National Laboratory, which is supported by the Office of Science of the U.S. Department of Energy under Contract No. DE-AC05-00OR22725. The authors thank helpful discussions and comments provided by Dr. Sang Soo Lee from Argonne National Laboratory.

References

1. Putnis, C. V.; Ruiz-Agudo, E., The Mineral-Water Interface: Where Minerals React with the Environment. *Elements* **2013**, *9*, 177-182.
2. Bruckenstein, S.; Shay, M., Experimental Aspects of Use of the Quartz Crystal Microbalance in Solution. *Electrochim. Acta* **1985**, *30*, 1295-1300.
3. Matsui, K.; Kikuma, J.; Tsunashima, M.; Ishikawa, T.; Matsuno, S. Y.; Ogawa, A.; Sato, M., In Situ Time-Resolved X-Ray Diffraction of Tobermorite Formation in Autoclaved Aerated Concrete: Influence of Silica Source Reactivity and Al Addition. *Cem. Concr. Res.* **2011**, *41*, 510-519.
4. Bell, J. L. S.; Palmer, D. A.; Barnes, H. L.; Drummond, S. E., Thermal-Decomposition of Acetate .3. Catalysis by Mineral Surfaces. *Geochimica Et Cosmochimica Acta* **1994**, *58*, 4155-4177.
5. Brown, G. E.; Calas, G., Mineral-Aqueous Solution Interfaces and Their Impact on the Environment. *Geochemical Perspectives* **2012**, *1*, 483-742.
6. Dove, P. M., The Dissolution Kinetics of Quartz in Aqueous Mixed Cation Solutions. *Geochimica Et Cosmochimica Acta* **1999**, *63*, 3715-3727.
7. Leung, K.; Criscenti, L. J.; Knight, A. W.; Ilgen, A. G.; Ho, T. A.; Greathouse, J. A., Concerted Metal Cation Desorption and Proton Transfer on Deprotonated Silica Surfaces. *Journal of Physical Chemistry Letters* **2018**, *9*, 5379-5385.
8. Rustad, J. R.; Wasserman, E.; Felmy, A. R.; Wilke, C., Molecular Dynamics Study of Proton Binding to Silica Surfaces. *Journal of Colloid and Interface Science* **1998**, *198*, 119-129.
9. Liu, X. D.; Cheng, J.; Lu, X. C.; Wang, R. C., Surface Acidity of Quartz: Understanding the Crystallographic Control. *Physical Chemistry Chemical Physics* **2014**, *16*, 26909-26916.
10. Ong, S. W.; Zhao, X. L.; Eisenthal, K. B., Polarization of Water-Molecules at a Charged Interface-2nd Harmonic Studies of the Silica Water Interface. *Chemical Physics Letters* **1992**, *191*, 327-335.
11. Du, Q.; Freysz, E.; Shen, Y. R., Vibrational-Spectra of Water-Molecules at Quartz Water Interfaces. *Physical Review Letters* **1994**, *72*, 238-241.
12. Higgins, S. R.; Stack, A. G.; Eggleston, C. M.; Afonso, M. D. S., Proton and Ligand Adsorption at Silica- and Alumina-Water Interfaces Studied by Optical Second Harmonic Generation (SHG). *Mineral. Mag.* **1998**, *62*, 616-617.
13. Dewan, S.; Yeganeh, M. S.; Borguet, E., Experimental Correlation between Interfacial Water Structure and Mineral Reactivity. *Journal of Physical Chemistry Letters* **2013**, *4*, 1977-1982.
14. Sulpizi, M.; Gaigeot, M. P.; Sprik, M., The Silica-Water Interface: How the Silanols Determine the Surface Acidity and Modulate the Water Properties. *Journal of Chemical Theory and Computation* **2012**, *8*, 1037-1047.
15. Leung, K.; Nielsen, I. M. B.; Criscenti, L. J., Elucidating the Bimodal Acid-Base Behavior of the Water-Silica Interface from First Principles. *J. Am. Chem. Soc.* **2009**, *131*, 18358-18365.

16. Bellucci, F.; Lee, S. S.; Kubicki, J. D.; Bandura, A.; Zhang, Z.; Wesolowski, D. J.; Fenter, P., Rb^+ Adsorption at the Quartz(101)-Aqueous Interface: Comparison of Resonant Anomalous X-Ray Reflectivity with Ab Initio Calculations. *Journal of Physical Chemistry C* **2015**, *119*, 4778-4788.
17. Schlegel, M. L.; Nagy, K. L.; Fenter, P.; Sturchio, N. C., Structures of Quartz (100)- and (101)-Water Interfaces Determined by X-Ray Reflectivity and Atomic Force Microscopy of Natural Growth Surfaces. *Geochimica Et Cosmochimica Acta* **2002**, *66*, 3037-3054.
18. Skelton, A. A.; Fenter, P.; Kubicki, J. D.; Wesolowski, D. J.; Cummings, P. T., Simulations of the Quartz(101)/Water Interface: A Comparison of Classical Force Fields, Ab Initio Molecular Dynamics, and X-Ray Reflectivity Experiments. *Journal of Physical Chemistry C* **2011**, *115*, 2076-2088.
19. Pfeiffer-Laplaud, M.; Gaigeot, M. P., Electrolytes at the Hydroxylated (0001) Alpha-Quartz/Water Interface: Location and Structural Effects on Interfacial Silanols by Dft-Based Md. *Journal of Physical Chemistry C* **2016**, *120*, 14034-14047.
20. Pfeiffer-Laplaud, M.; Gaigeot, M. P.; Sulpizi, M., Pk(a) at Quartz/Electrolyte Interfaces. *Journal of Physical Chemistry Letters* **2016**, *7*, 3229-3234.
21. Elstner, M.; Frauenheim, T.; Kaxiras, E.; Seifert, G.; Suhai, S., A Self-Consistent Charge Density-Functional Based Tight-Binding Scheme for Large Biomolecules. *Physica Status Solidi B-Basic Solid State Physics* **2000**, *217*, 357-376.
22. Cui, Q.; Elstner, M., Density Functional Tight Binding: Values of Semi-Empirical Methods in an Ab Initio Era. *Physical Chemistry Chemical Physics* **2014**, *16*, 14368-14377.
23. Koskinen, P.; Makinen, V., Density-Functional Tight-Binding for Beginners. *Computational Materials Science* **2009**, *47*, 237-253.
24. Aradi, B.; Hourahine, B.; Frauenheim, T., DFTB+, a Sparse Matrix-Based Implementation of the DFTB Method. *Journal of Physical Chemistry A* **2007**, *111*, 5678-5684.
25. Gaus, M.; Cui, Q. A.; Elstner, M., Dftb3: Extension of the Self-Consistent-Charge Density-Functional Tight-Binding Method (SCC-DFTB). *Journal of Chemical Theory and Computation* **2011**, *7*, 931-948.
26. Bandura, A. V.; Kubicki, J. D.; Sofo, J. O., Periodic Density Functional Theory Study of Water Adsorption on the Alpha-Quartz (101) Surface. *Journal of Physical Chemistry C* **2011**, *115*, 5756-5766.
27. Guimaraes, L.; Enyashin, A. N.; Frenzel, J.; Heine, T.; Duarte, H. A.; Seifert, G., Imogolite Nanotubes: Stability, Electronic, and Mechanical Properties. *Acs Nano* **2007**, *1*, 362-368.
28. Dftb.Org
29. Goyal, P.; Qian, H. J.; Irle, S.; Lu, X. Y.; Roston, D.; Mori, T.; Elstner, M.; Cui, Q., Molecular Simulation of Water and Hydration Effects in Different Environments: Challenges and Developments for DFTB Based Models. *Journal of Physical Chemistry B* **2014**, *118*, 11007-11027.
30. Bunker, B. C.; Haaland, D. M.; Ward, K. J.; Michalske, T. A.; Smith, W. L.; Binkley, J. S.; Melius, C. F.; Balfe, C. A., Infrared-Spectra of Edge-Shared Silicate Tetrahedra. *Surface Science* **1989**, *210*, 406-428.
31. Fenter, P.; Kerisit, S.; Raiteri, P.; Gale, J. D., Is the Calcite-Water Interface Understood? Direct Comparisons of Molecular Dynamics Simulations with Specular X-Ray Reflectivity Data. *Journal of Physical Chemistry C* **2013**, *117*, 5028-5042.
32. Zhang, Z., et al., Ion Adsorption at the Rutile-Water Interface: Linking Molecular and Macroscopic Properties. *Langmuir* **2004**, *20*, 4954-4969.
33. Harmon, K. J.; Chen, Y.; Bylaska, E. J.; Catalano, J. G.; Bedzyk, M. J.; Weare, J. H.; Fenter, P., Insights on the Alumina Water Interface Structure by Direct Comparison of Density Functional Simulations with X-Ray Reflectivity. *Journal of Physical Chemistry C* **2018**, *122*, 26934-26944.
34. Bracco, J. N.; Lee, S. S.; Stubbs, J. E.; Eng, P. J.; Heberling, F.; Fenter, P.; Stack, A. G., Hydration Structure of the Barite (001)-Water Interface: Comparison of X-Ray Reflectivity with Molecular Dynamics Simulations. *Journal of Physical Chemistry C* **2017**, *121*, 12236-12248.
35. Stack, A. G.; Stubbs, J. E.; Srinivasan, S. G.; Roy, S.; Bryantsev, V. S.; Eng, P. J.; Custelcean, R.; Gordon, A. D.; Hexel, C. R., Mineral-Water Interface Structure of Xenotime (Ypo4) {100}. *Journal of Physical Chemistry C* **2018**, *122*, 20232-20243.
36. Rivera, L. O.; Bakaev, V. A.; Banerjee, J.; Mueller, K. T.; Pantano, C. G., Characterization and Reactivity of Sodium Aluminoborosilicate Glass Fiber Surfaces. *Applied Surface Science* **2016**, *370*, 328-334.
37. Sanders, R. L.; Washton, N. M.; Mueller, K. T., Measurement of the Reactive Surface Area of Clay Minerals Using Solid-State Nmr Studies of a Probe Molecule. *Journal of Physical Chemistry C* **2010**, *114*, 5491-5498.
38. Macias-Romero, C.; Nahalka, I.; Okur, H. I.; Roke, S., Optical Imaging of Surface Chemistry and Dynamics in Confinement. *Science* **2017**, *357*, 784-787.

39. Fenter, P. A., X-Ray Reflectivity as a Probe of Mineral-Fluid Interfaces: A User Guide. In *Applications of Synchrotron Radiation in Low-Temperature Geochemistry and Environmental Sciences*, Fenter, P. A.; Rivers, M. L.; Sturchio, N. C.; Sutton, S. R., Eds. 2002; Vol. 49, pp 149-220.

TOC Graphic